energies

Article

Unsteady Magnetohydrodynamic Radiative Casson Nanofluid within Chemically Reactive Flow over a Stretchable Surface with Variable Thickness through a Porous Medium

Ahmed M. Sedki [1,*] and Raed Qahiti [2]

[1] Department of Mathematics, Faculty of Science, Ain Shams University, Cairo 11566, Egypt
[2] Department of Mathematics, Faculty of Science, Jazan University, Jazan 45142, Saudi Arabia; rqahiti@jazanu.edu.sa
* Correspondence: a.m.sedki@hotmail.com

Abstract: This study presents a mathematical investigation into the phenomena of radiative heat with an unsteady MHD electrically conducting boundary layer of chemically reactive Casson nanofluid flow due to a pored stretchable sheet immersed in a porous medium in the presence of heat generation, thermophoretic force, and Brownian motion. The surface is assumed to be not flat, and has variable thickness. The magnetic field is time-dependent, and the chemical reaction coefficient is inversely varied with the distance. The nanofluid's velocity, heat, and concentration at the surface are nonlinearly varied. A similarity transformation is introduced, and the controlling equations are converted into nondimensional forms involving many significant physical factors. The transformed forms are analyzed numerically using a computational method based on the finite difference scheme and Newton's linearization procedure. The impact of the involved physical parameters is performed in graphical and tabular forms. Some special cases of the current work are compared with published studies, and an excellent agreement is obtained. The main results of the present work indicate that the higher values of the Casson parameter cause an increase in both the shear stress and heat flux, but a decrease in the mass flux. Also, it is noted that the chemical reaction, the nanoparticles' volume, and the permeability factor enhance the effect the of Casson parameter on both the shear stress and heat flux, while the variable thickness and thermal radiation field reduce it; on the other hand, the variable thickness and nanoparticles' volume enforce the influence of the Casson parameter on mass flux, but thermal radiation, the permeability factor, and chemical reaction decrease it. The present study has important applications in mechanical engineering and natural sciences. In addition, it has significant applications in devices used for blood transfusion, dialysis and cancer therapy.

Keywords: Casson nanofluid; thermal radiation; surface variable thickness; porous medium; chemical reaction; thermophoretic force; Brownian motion

Citation: Sedki, A.M.; Qahiti, R. Unsteady Magnetohydrodynamic Radiative Casson Nanofluid within Chemically Reactive Flow over a Stretchable Surface with Variable Thickness through a Porous Medium. *Energies* **2023**, *16*, 7776. https://doi.org/10.3390/en16237776

Academic Editors: Roger Gläser, Kyung Chun Kim, Belal Dawoud and Artur Blaszczuk

Received: 1 July 2023
Revised: 14 November 2023
Accepted: 20 November 2023
Published: 25 November 2023

1. Introduction

Convective heat through nanofluid flow enhances the surface characteristics of materials by improving the mechanical strength, thermal conductivity, and electromagnetic efficiency, and is a noticed phenomenon. Its importance has been reported in various industrial applications and new biotechnologies. Therefore, many authors are interested in analyzing the characteristics of heat convection in nanofluid flow problems [1,2]. Elbashbeshy [3] investigated the features of unsteady convective heat in the nanofluid flow over a stretchable sheet. Ishak [4] analyzed the influence of a magnetic field on an unsteady convective heat in the fluid flowing over a stretchable sheet with variable velocity and temperature. Ibrahim [5] investigated the characteristics of MHD convective heat in an unsteady fluid flow over a stretchable surface considering the heat generation effect. Makinde et al. [6] studied the thermal radiative and magnetic field effects on convective heat in variable viscosity fluid flowing over a nonlinear heated surface and taking into consideration the thermophoretic force. Sheikholeslami [7] reported the feature of thermal radiation in an unsteady natural convective through nanofluid flow considering the magnetic field. Elbashbeshy et al. [8] studied the impact of thermal radiation on convective heat in viscous fluid flow around a thermal sphere immersed in a porous medium considering Newtonian heat. Eldabe et al. [9] considered the chemically reactive flow of non-Newtonian nanofluid with convective heat over a stretchable sheet in the existing magnetic field. Trivedi et al. [10] studied the magneto-mixed convective heat in nanofluid flow with heat generation. Mahabaleshwar et al. [11] investigated the magnetohydrodynamic-induced fluid flow and mass transfer over a nonlinearly extendable sheet. Khan et al. [12] examined the influence of Dufour and Soret on an electrically conducting non-Newtonian fluid in the existence of a variable magnetic field. Maleki et al. [13] analyzed the properties of convective heat in nanofluid flow over a permeable sheet considering radiative heat and slip boundary conditions. Prodanjani et al. [14] investigated the impacts of thermal radiative heat on magnetoconvective heat transfer in nanofluid flow in a cavity. Chaudhary et al. [15] performed an investigation on heat generation and radiative heat effects on the MHD nanofluid flow of a stagnation point for a heated extendable sheet. Reddy et al. [16] investigated the behavior of heat convective in a reactive flow of nanofluid over an inclined plate immersed in a porous media. Eldabe et al. [17] examined the impact of the magnetic field on a peristaltic flow of non-Newtonian nanofluid embedded in an inclined channel that was immersed in a non-Darcy porous medium. Sedki et al. [18] presented a study on thermal radiative and heat generation effects on an unsteady mixed convective heat in nanofluid flow due to a stretchable surface embedded in porous. The thermophoretic forces, Brownian motion, and surface flow flux are considered. Sedki [19] reported the impacts of thermal radiation on a magneto-mixed convective heat in a reactive flow of steady nanofluid due to a nonlinearly stretchable surface in a porous medium considering a chemical reaction.

Non-Newtonian fluid has various applications in industrial engineering and modern technology. Casson fluid is a characteristic of non-Newtonian fluid and it is sometimes called viscoelastic fluid. Human blood, honey, tomato sauce, and jelly are examples of the Casson fluid. Due to its significant applications, several researchers are focused on the analysis of the Casson fluid behavior. The behavior of Casson fluid flow in an unsteady boundary layer over a stretching surface was investigated by Mukhopadhyay [20]. The shooting numerical scheme is used in solving the involved equations. Makanda et al. [21] performed an investigation on chemical reactive species through unsteady Casson fluid due to stretching surface in a porous medium in the existence of magnetic field effects. The study was analyzed by the Runge–Kutta–Felhberg numerical method. Raju et al. [22] reported the behavior of convective heat in MHD Casson fluid flowing in a porous exponentially stretchable surface considering thermal radiation and chemical reactive flow. Oyelakin et al. [23] reported the characteristics of unsteady Casson fluid flow over a stretchable surface in the existence of radiative heat and heat source/sink. The effect of thermophoresis and Brownian motion are discussed. Krishnamurthy et al. [24] presented a theoretical investigation to discuss the thermal radiation effect on the MHD nanofluid flow through a nonlinearly stretchable sheet. Numerical investigation of thermal radiation on magneto Casson fluid flow, due to an unsteady stretchable sheet immersed in a porous medium considering the heat generation impacts, was introduced by Ullah et al. [25]. Prasad et al. [26] considered the steady Casson nanofluid flow over a stretchable plane with variable thickness considering the magnetic field effect. Tamoor et al. [27] analyzed the magnetic field effect on Casson fluid flowing over a linear stretched cylinder. Naqvi et al. [28] investigated the properties of Casson fluid flow containing nanoparticles over a moving cylinder with thermal radiation and a magnetic field. Shit and Mandal [29] analyzed the behavior of unsteady Casson nanofluid flow due to a moving vertical surface considering thermal radiation and magnetic field. Krishna et al. [30] reported the characteristic of radiative heat in the MHD Casson hybrid nanofluid due to an accelerated vertical permeable surface. Bejawada et al. [31] numerically studied the influence of thermal radiation on a magneto Casson fluid over an inclined surface through a porous medium. Sedki [32] considered the thermal radiative heat and chemically reactive flow of MHD cross nanofluid containing gyrotactic microorganisms due to a permeable horizontal cylinder through a porous medium. Khan et al. [33] examined a magneto-Williamson hybrid nanofluid flow through a thin vertical needle. Joule heating and viscous dissipation were discussed. Further, the impact of thermal radiation and homogeneous reaction were also taken into consideration.

In this study, according to the above literature review, we are interested in analyzing the impact of thermal radiation on the chemically reactive flow of an unsteady electrically conducting MHD Casson nanofluid over a permeable stretchable surface with variable thickness immersed in a porous medium. Furthermore, the heat generation, thermophoretic force, and Brownian motion effects are also taken into account. The surface is assumed to be not flat, and its thickness is time-dependent. The convective boundary conditions of the nanofluid at the porous surface are nonlinearly varying with time and distance.

2. Analysis and Formulation of the Problem

We consider the unsteady MHD-mixed convective through a two-dimensional chemical reactive as an incompressible, viscous Casson nanofluid immersed in a porous medium along a permeable surface. The surface stretches nonlinearly with velocity $U_w(x,t)$, $U_w(x,t) = ax/1 - \Gamma t$. The coordinates (x, y) are chosen in which the x axis is taken along the sheet. However, the y axis is normal to it. The fluid is electrically conducting due to the existing variable magnetic field, which is perpendicular to the sheet, $B(t) = B_0(1 - \Gamma t)^{-1/2}$ [Tesla], where B_0 is a constant. In the absence of an electric field, the electromagnetic Lorentz force is determined as $\vec{F} = \vec{J} \times \vec{B}$, $\vec{J} = \sigma_{nf}(\vec{V} \times \vec{B})$, where $\vec{J}$ is the electric current, and $\vec{V}$ denotes the vector of the velocity. The magnetic Reynolds number is assumed to be low, so the induced magnetic field is negligible.

The surface is assumed to be not flat and has variable thickness, which is defined as $y = \delta\sqrt{(1 - \Gamma t)}$, $\Gamma t \le 1$; δ is small and so the surface is sufficiently thin. The selected geometry has very strong applications in industrial engineering, such as in the extrusion of a polymer, the process of liquid film condensation, coating emulsion on photographic films, melt-spinning, and hot rolling. Also, it is used in mechanical marine and aerospace industries. The physical flow and the system's coordinates are drawn in Figure 1.

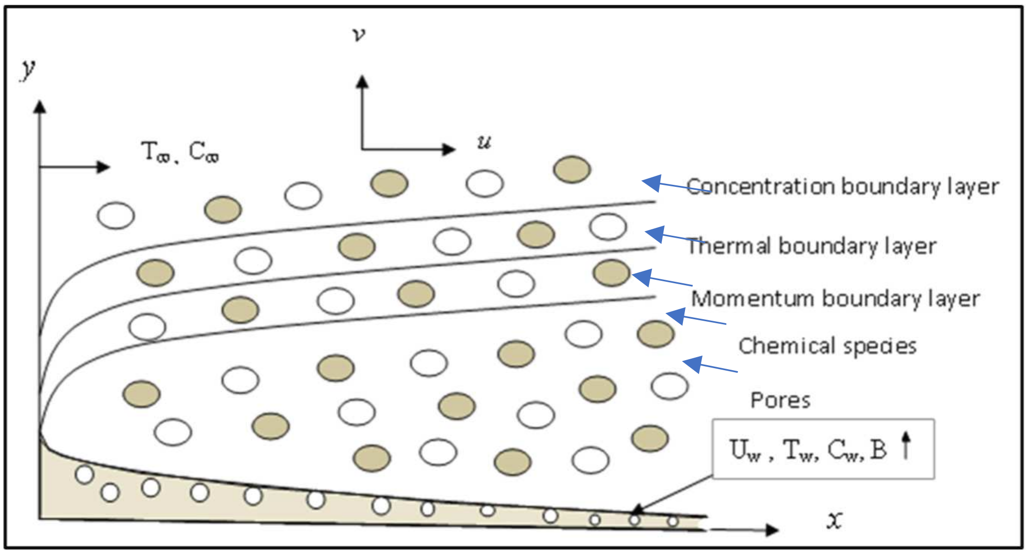

Figure 1. Schematic of the problem.

The rheological state equation for the Casson fluid flow is given as [20,21]

$$\tau_{ij} = \begin{cases} 2(\mu_B + P_y/\sqrt{2\pi})e_{ij} & \pi > \pi_c \\ 2(\mu_B + P_y/\sqrt{2\pi})e_{ij} & \pi < \pi_c \end{cases} \tag{1}$$

where $\pi = e_{ij}e_{ij}$.

In the existence of thermal radiation, thermophoretic force, Brownian motion, heat generation, and variable magnetic field, the governing equations of this model are given by [20–25].

$$\frac{\partial u}{\partial x} + \frac{\partial v}{\partial y} = 0 \tag{2}$$

$$\frac{\partial u}{\partial t} + u\frac{\partial u}{\partial x} + v\frac{\partial u}{\partial y} = v_{nf}\left(1 + \frac{1}{\beta}\right)\frac{\partial^2 u}{\partial y^2} - \frac{\sigma_{nf} B^2(t)}{\rho_{nf}}u + g(\beta_{nf})_T(T - T_\infty) + g(\beta_{nf})_C(C - C_\infty) - \frac{v_{nf}}{k_p}u \tag{3}$$

$$\begin{aligned} \frac{\partial T}{\partial t} + u\frac{\partial T}{\partial x} + v\frac{\partial T}{\partial y} = \; & \frac{k_{nf}}{(\rho C_P)_{nf}}\frac{\partial^2 T}{\partial y^2} + \tau\left[D_B\left(\frac{\partial T}{\partial y}\frac{\partial C}{\partial y}\right) + \frac{D_T}{T_\infty}\left(\frac{\partial T}{\partial y}\right)^2\right] + \\ & \frac{\mu_{nf}}{(\rho c_P)_{nf}}\left(1 + \frac{1}{\beta}\right)\left(\frac{\partial u}{\partial y}\right)^2 + \frac{Q}{(\rho C_P)_{nf}}(T - T_\infty) - \frac{1}{(\rho C_P)_{nf}}\frac{\partial q_r}{\partial y} \end{aligned} \tag{4}$$

$$\frac{\partial C}{\partial t} + u\frac{\partial C}{\partial x} + v\frac{\partial C}{\partial y} = D_B\frac{\partial^2 C}{\partial y^2} + \frac{D_T}{T_\infty}\frac{\partial^2 T}{\partial y^2} + R(C - C_\infty) \tag{5}$$

where $\tau = \frac{(\rho C_P)_p}{(\rho C_P)_f}$, $\beta = \mu_B\sqrt{2\pi_c}/P_y$.

Here, T and C are the nanofluid's temperature and concentration. u and v represent the x-component and y-component of the nanofluid's velocity, the time is assigned by t, and the gravity field is by g [m s^{-2}]. Also, R, q_r, and Q are the chemical reaction coefficient, the radiative heat flux, and the heat source, respectively. The coefficient of permeability of a porous medium is denoted by k_p, $k_p = k_0(1 - \Gamma t)$, where k_0 is the initial permeability. μ, ρ, k, and σ are the dynamic viscosity, the density, the effective thermal conductivity, and the electrical conductivity, respectively. The indices f, s, and nf are pointed to the base liquid, the nanoparticles, and the nanofluid, respectively. The specific heat at a fixed pressure is assigned by C_p, the coefficient of thermal expansion by β_T, the Brownian motion diffusion by D_b, and the thermophoretic diffusion by D_T. The nanoparticles are considered to be spherical and their volume fraction is represented by ϕ, the parameter of the Casson fluid by β, and τ is the ratio of the effective heat capacity of the nanoparticle to that of the fluid. The copper nanoparticles and the base liquid (water) properties are considered as in Sedki [18]. The characteristics of the nanofluid, base liquid, and solid nanoparticles are determined by

$$\begin{aligned} & \mu_{nf} = \frac{\mu_f}{(1-\phi)^{2.5}}, \rho_{nf} = (1 - \phi)\rho_f + \phi\rho_s, \alpha_{nf} = \frac{k_{nf}}{(\rho C_p)_{nf}} \\ & (\rho\beta_T)_{nf} = (1 - \phi)(\rho\beta_T)_f + \phi(\rho\beta_T)_s, \ (\rho C_P)_{nf} = (1 - \phi)(\rho C_P)_f + \phi(\rho C_P)_s \\ & k_{nf} = \left[\frac{(k_s+2k_f)+2(k_s-k_f)\phi}{(k_s+2k_f)-(k_s-k_f)\phi}\right]k_f, \ \sigma_{nf} = \left[\frac{(\sigma_s+2\sigma_f)+2(\sigma_s-\sigma_f)\phi}{(\sigma_s+2\sigma_f)-(\sigma_s-\sigma_f)\phi}\right]\sigma_f \end{aligned} \tag{6}$$

$$(\beta_c)_{nf} = \frac{1}{\rho_{f_\infty}}\frac{\partial\rho}{\partial C}|_{T_\infty,P_\infty} \simeq \frac{1}{\rho_{f_\infty}}\frac{\rho_s - \rho_{f_\infty}}{1 - C_\infty} \tag{7}$$

Here, ρ_{f_∞}, T_∞, and P_∞ are the nanofluid ambient density, temperature, and pressure, respectively. The appropriate boundary conditions are

$$\begin{aligned} & u = U_w, \ v = V_w, \ T = T_w \text{ , and } \mathrm{C} = \mathrm{C_w} \ at \ y = y_c = \delta\sqrt{(1 - \Gamma t)} \\ & u = 0, T \to T_\infty \text{ and } C \to C_\infty asy \ \to \infty \end{aligned} \tag{8}$$

where

$$U_w = \frac{ax}{1-\Gamma t},\ T_w = T_\infty + \frac{E_1 x^m}{(1-\Gamma t)^n},\ \text{and } C_w = C_\infty + \frac{E_2 x^m}{(1-\Gamma t)^n} \tag{9}$$

Here, V_w is the velocity of the suction (injection) ($V_w > 0$ for the suction and $V_w < 0$ for the injection), the fluid kinematic viscosity is denoted by ν_f and the ambient temperature by $T_\infty \cdot a$ and Γ are constants with dimension time^{-1}, where $a > 0$, $\Gamma \geq 0$, and $\Gamma t < 1$. E_1 and E_2 are constants with dimension temperature·length^{-1}. The positive values of E_1 and E_2 are considered for assisting flows, but negative values are for opposing flows where natural convection is considered when $E_1 = 0$ and $E_2 = 0$. The fluid is postulated to be grey and the radiation approximation presented by Rosseland has been applied, and then the radiative heat flux is determined by

$$q_r = -\frac{4\sigma^*}{3k_1}\frac{\partial T^4}{\partial y} \tag{10}$$

Here, σ^* is the Stefan–Boltzman constant and k_1 denotes the coefficient of mean absorption. Taylor series is applied to expand T^4 about T_∞, and when the higher order terms are neglected, we obtain $T^4 = 4T_\infty^3 T - 3T_\infty^4$. By substituting into Equation (7), we obtain

$$q_r = -\frac{16\sigma^* T_\infty^3}{3k_1}\frac{\partial T}{\partial y} \tag{11}$$

For a similarity solution, we put

$$\eta = y\sqrt{\frac{\mathrm{a}}{\nu_{nf}(1-\Gamma t)}},\ \psi = \sqrt{\frac{\mathrm{a}\nu_{nf}}{(1-\Gamma t)}}xF(\eta),\ \Theta(\eta) = \frac{T-T_\infty}{T_w - T_\infty}, and\ \Phi(\eta) = \frac{C-C_\infty}{C_w - C_\infty} \tag{12}$$

Here, η represents the variable of similarity, ψ denotes the stream function, Θ is the nanofluid dimensionless temperature, and Φ denotes the nanofluid dimensionless concentration. By substitution in the governing Equations (2)–(5), we have

$$\begin{aligned}\left(1+\tfrac{1}{\beta}\right)F^{\backslash\backslash\backslash} + \left(\tfrac{\rho_{nf}}{\rho_f}/\tfrac{\mu_{nf}}{\mu_f}\right)\left[F.F^{\backslash\backslash} - F^{\backslash 2} - A\left(F^{\backslash} + \tfrac{\eta}{2}F^{\backslash\backslash}\right)\right] - \left(\tfrac{\sigma_{nf}}{\sigma_f}/\tfrac{\mu_{nf}}{\mu_f}\right)M\,F^{\backslash} \\ +\left(\tfrac{Gr_T}{Re_x^2}\left(\tfrac{(\rho\beta_T)_{nf}}{(\rho\beta_T)_f}/\tfrac{\mu_{nf}}{\mu_f}\right)\Theta + \left(\tfrac{Gr_C}{Re_x^2}/\tfrac{\mu_{nf}}{\mu_f}\right)\Phi\right) - K\,F^{\backslash} = 0\end{aligned} \tag{13}$$

$$\begin{aligned}\tfrac{1}{\Pr}\left(\tfrac{k_{nf}}{k_f} + \tfrac{4}{3}Rd\right)\Theta^{\backslash\backslash} + \tfrac{(\rho c_p)_{nf}}{(\rho c_p)_f}\left[F.\Theta^{\backslash} - m\,F^{\backslash}.\Theta - A\left(n.\Theta + \tfrac{\eta}{2}\Theta^{\backslash}\right)\right] + \lambda\Theta \\ +\tfrac{(\rho c_p)_{nf}}{(\rho c_p)_f}\left[Nb.\Theta^{\backslash}.\Phi^{\backslash} + Nt.\Theta^{\backslash^2}\right] + \tfrac{\mu_{nf}}{\mu_f}\left(1+\tfrac{1}{\beta}\right)EcF^{\backslash\backslash^2} = 0\end{aligned} \tag{14}$$

$$\frac{D_B}{v_\rho}\Phi^{\backslash\backslash} + F.\Phi^{\backslash} - m\,F^{\backslash}.\Phi - A\left(n\Phi + \frac{\eta}{2}\Phi^{\backslash}\right) + \frac{D_T}{v_\rho}\frac{Nb}{Nt}\Theta^{\backslash\backslash} - \left(\frac{xR}{U_w}\right)\Phi = 0 \tag{15}$$

and boundary conditions become

$$\begin{aligned}F(\eta) = -V_w\sqrt{\tfrac{x}{U_w \nu_{nf}}},\ F^{\backslash}(\eta) = 1,\ \Theta(\eta) = 1,\ \text{and } Nb.\Phi^{\backslash}(\eta) + Nt.\Theta^{\backslash}(\eta) = 0 \text{ at } \eta = \gamma = \delta\sqrt{\tfrac{\nu_{nf}}{a}} \\ F(\eta) = 0, F^{\backslash}(\eta) = 0, \Theta(\eta) = 0,\ \text{and } \Phi(\eta) = 0 \text{ as } \eta \to \infty\end{aligned} \tag{16}$$

The ratio Gr/Re^2 is important in the heat convective and mass transfer correlation. Forced convection is taken into consideration when $Gr/Re^2 >> 1$, while natural convection is considered for $Gr/Re^2 << 1$. The mixed convection is taken into account when Gr/Re^2 is of order one (for more details see, Sedki [18]).

The surface is considered not flat, and its thickness varies nonlinearly with the time t. We put $z = \eta - \gamma$, then $F(z) = F(\eta - \gamma) = f(\eta)$

Consider

$$\eta = z + \gamma,\ f(\eta) = F(z),\ \theta(\eta) = \Theta(z),\ \text{and } C(\eta) = \Phi(z) \tag{17}$$

Now Equations (13)–(15) and the appropriate conditions (16) become

$$\left(1+\frac{1}{\beta}\right)f^{\backslash\backslash\backslash} + A_1\left(f.f^{\backslash\backslash} - f^{\backslash 2} - A\left(f^{\backslash} + \frac{z+\gamma}{2}f^{\backslash\backslash}\right)\right) - MA_2\, f^{\backslash} + (A_3\alpha.\theta + A_4\delta.C) - Kf^{\backslash} = 0 \tag{18}$$

$$\frac{1}{\Pr}\left(1+\frac{4}{3}Rd\right)\theta^{\backslash\backslash} + A_5\left(f.\theta^{\backslash} - m\, f^{\backslash}.\theta - A\left(n.\theta + \frac{z+\gamma}{2}\theta^{\backslash}\right) + Nb.\theta^{\backslash}C^{\backslash} + Nt.\theta^{\backslash 2}\right) + \lambda\theta + A_4\left(1+\frac{1}{\beta}\right)Ecf^{\backslash\backslash 2} = 0 \tag{19}$$

$$\frac{1}{Sc}C^{\backslash\backslash} + f.C^{\backslash} - m\, f^{\backslash}.C - A\left(nC + \frac{z+\gamma}{2}C^{\backslash}\right) + \frac{1}{Sc}\frac{N_b}{N_t}\theta^{\backslash\backslash} - R_c\, C = 0 \tag{20}$$

$$\begin{gathered} f(0) = f_w,\ f^{\backslash}\,(0) = 1, \theta\Big(0\Big) = 1,\ Nb.C^{\backslash}(0) + Nt.\theta^{\backslash}(0) = 0 \text{ at } \eta = 0 \\ f^{\backslash}(\eta) = 0, \theta(\eta) = 0, \text{ and } C(\eta) = 0 \text{ as } \eta \to\ \infty \end{gathered} \tag{21}$$

where A is the unsteadiness factor, M is the magnetic factor and Pr denotes the Prandtl number. Ec assigns Eckert number, and fw is the surface flow flux parameter (it represents a suction when $fw > 0$ and injection when $fw < 0$), The thermal diffusion is assigned by α, the mass diffusion by δ, K denotes porosity parameter, Nt is the thermophoretic parameter, and Nb is the Brownian motion parameter, Pr is the Prandtl number, Sc denotes the Schmidt number, λ assigns the heat generation factor (it represents heat source when $\lambda > 0$ and heat sink when $\lambda < 0$), and Rc assigns the parameter of the chemical reaction. These are given by

$$A = \frac{\Gamma}{a},\ \alpha = \left(\frac{Gr_T}{Re_x^2}\right), \delta = \left(\frac{Gr_C}{Re_x^2}\right),\ M = \frac{\sigma_f\beta_0^2}{a\rho_f}, K = \frac{k_0}{a},\ \lambda = \frac{Q_0 x}{U_w(\rho c_p)_f},\ Rd = \left(\frac{4\sigma^* T_\infty^3}{3\alpha k_f}\right)$$

$$\Pr = \frac{\alpha_f}{\nu_f},\ \mathrm{Re}_x = \frac{xU_w}{\upsilon_f}, Gr_T = \frac{g(\beta_T)_f(T_w - T_\infty)x^3}{\nu_f^2}, Gr_C = \frac{g(\rho_s - \rho_f)(C_w - C_\infty)x^3}{\rho_f(1-C_\infty)\,\nu_f^2},\ Sc = \frac{\nu_f}{D_B}$$

$$Rc = \frac{Rx}{U_w},\ fw = -V_w\sqrt{\left(\frac{x}{\nu_f U_w}\right)},\ Nt = \frac{\tau D_T(T_w - T_\infty)}{\nu_f T_\infty},\ Nb = \frac{\tau D_B(C_w - C_\infty)}{\nu_f}, Ec = \frac{U_w^2}{(T_w - T_\infty)c_p}$$

$$\begin{gathered} A_1 = (1-\phi)^{2.5}\left((1-\phi) + \phi\tfrac{\rho_s}{\rho_f}\right),\ A_2 = (1-\phi)^{2.5}\left[\tfrac{(\sigma_s+2\sigma_f)+2(\sigma_s-\sigma_f)\phi}{(\sigma_s+2\sigma_f)-(\sigma_s-\sigma_f)\phi}\right] \\ A_3 = (1-\phi)^{2.5}\left((1-\phi) + \phi\tfrac{(\rho\beta_T)_s}{(\rho\beta_T)_f}\right), A_4 = (1-\phi)^{2.5}, A_5 = \left[(1-\phi) + \phi\tfrac{(\rho C_P)_s}{(\rho C_P)_f}\right] \end{gathered} \tag{22}$$

The important quantities of interest for this problem are the skin friction Cf [N·m^{-2}] and Nusselt number Nu, and the Sherwood number Sh_x. They indicate, physically, the surface shear stress τ_w, surface heat flux q_w, and mass flux q_c, respectively, and are given by

$$Cf = \frac{\tau_w}{\rho_f U_w^2}, Nu = \frac{xq_w}{k_f(T_w - T_\infty)},\ \mathrm{Sh} = \frac{xq_c}{D_B(C_w - C_\infty)} \tag{23}$$

where τ_w, q_w, and q_c are given by

$$\tau_w = \mu_{nf}\left(1+\frac{1}{\beta}\right)\left(\frac{\partial u}{\partial y}\right)_{y=y_c} = \mu_{nf}\left(1+\frac{1}{\beta}\right)\frac{ax}{(1-\gamma t)}\sqrt{\frac{a}{\upsilon_f(1-\gamma t)}}F^{\backslash\backslash}(\eta)|_{\eta=\gamma} = \mu_{nf}U_w\left(1+\frac{1}{\beta}\right)\sqrt{\frac{U_w}{\upsilon_f x}}f^{\backslash\backslash}(0) \tag{24}$$

$$q_w = -k_{nf}\left(\frac{\partial T}{\partial y}+q_r\right)_{y=y_c} = -(T_w-T_\infty)\sqrt{\frac{a}{\upsilon_f(1-\gamma t)}}\left(\frac{k_{nf}}{k_f}+\frac{4}{3}Rd\right)\Theta^{\backslash}(\eta)|_{\eta=\gamma} = -(T_w-T_\infty)\sqrt{\frac{U_w}{x\upsilon_f}}\left(\frac{k_{nf}}{k_f}+\frac{4}{3}Rd\right)\Theta^{\backslash}(\eta) \tag{25}$$

$$q_m = -D_B\left(\frac{\partial C}{\partial y}\right)_{y=y_c} = -D_B(C_w-C_\infty)\sqrt{\frac{a}{\upsilon_f(1-\gamma t)}}\Phi^{\backslash}(\eta)|_{\eta=\gamma} = -D_B(C_w-C_\infty)\sqrt{\frac{U_w}{x\upsilon_f}}C^{\backslash}(0) \tag{26}$$

Now we get

$$Cf\sqrt{\mathrm{Re}_x} = \frac{\mu_{nf}}{\mu_f}\left(1+\frac{1}{\beta}\right)f^{\backslash\backslash}(0), Nu/\sqrt{\mathrm{Re}_x} = -\left(\frac{k_{nf}}{k_f}+\frac{4}{3}Rd\right)\theta^{\backslash}(0), Sh/\sqrt{\mathrm{Re}_x} = -C^{\backslash}(0) \tag{27}$$

3. Numerical Results

The basic equations controlling the study (2)–(7) are converted into similarity forms (18)–(21) that involve many significant physical parameters. The study is computationally analyzed by developing a Matlab algorithm composed of the finite difference scheme with Newton's linearization procedure. For validation of the computational results, a comparison is presented in Table 1 for special cases of current work with the published results introduced by Elbashbeshy [3], Ishak [4], and Ibrahim [5], and good agreement is obtained. The fixed values of the physical parameters in the current analysis are considered as Pr = 10, β = 0.5, ϕ = 0.05, At = 0.1, Nt = 0.5, fw = 1, Sc = 10.0, Rd = 0.5, λ = 0.2, α = 0.5, Rc = 0.2, K = 0.2, Ec = 0.5, Nb = 0.5, γ = 0.1, m = 1, n = 1.

Table 1. A comparison of the present results of $-\theta^{\backslash}(0)$ for Pr values with M = 0, n = 1, m = 1, ϕ = 0, and λ = 0.0 with that reported by Elbasbeshy [3], Ishak [4], and Ibrahim [5].

Pr	Elbashbeshy [3]	Ishak [4]	Ibrahim [5]	Present Study	
	$-\theta^{\backslash}(0)$	$-\theta^{\backslash}(0)$	$-\theta^{\backslash}(0)$	$-f^{\backslash\backslash}(0)$	$-\theta^{\backslash}(0)$
0.72	0.808	0.8086	0.8095	1.0000	0.80864
1.0	1.0	1.0	1.0001	1.0000	1.0000
10	3.7207	3.7202	3.7208	1.0000	3.7207

The numerical results showing the impacts of the physical factors involved in the nondimensional equations for the nanofluid's velocity, temperature, and mass concentration profiles are performed in graphical forms (2)–(12), while the impacts of the involved parameters on shear stress, heat flux, and mass flux are presented in tabular forms (2)–(5). The impact of the Casson parameter is performed in Figure 2a–c. It is shown that the increase in the Casson parameter causes acceleration in the concentration, but the inverse results in velocity and temperature occurring near the wall. Physically it is due to the increasing values of the Casson parameter enhancing the viscous forces, which delays the flow and therefore reduces the nanofluid velocity. The effect of surface thickness γ is performed in Figure 3a–c. It is noted that the increase in variable thickness factor causes an increase in both the nondimensional velocity $f^{\backslash}$ and temperature profiles, but the inverse effect happens on temperature near the wall. Also, the increase in the variable thickness parameter causes a decrease in the concentration C. The impacts of thermal radiation are shown graphically in Figure 4a–c. It is noted that the higher values in thermal radiation cause an increase in both the nondimensional velocity $f^{\backslash}$ and temperature. Also, it is noted from Figure 4c that the accelerated values of thermal radiation cause an increase in the concentration, but the opposite effect occurs far from the wall. The impact of the permeability parameter *fw* is presented graphically in Figure 5a–c. It is noted that the increase in the permeability of the surface *fw* causes a decrease in both the nondimensional velocity and temperature. Also, the rising *fw* results in a decrease in the concentration, but the effect is changed far from the wall.

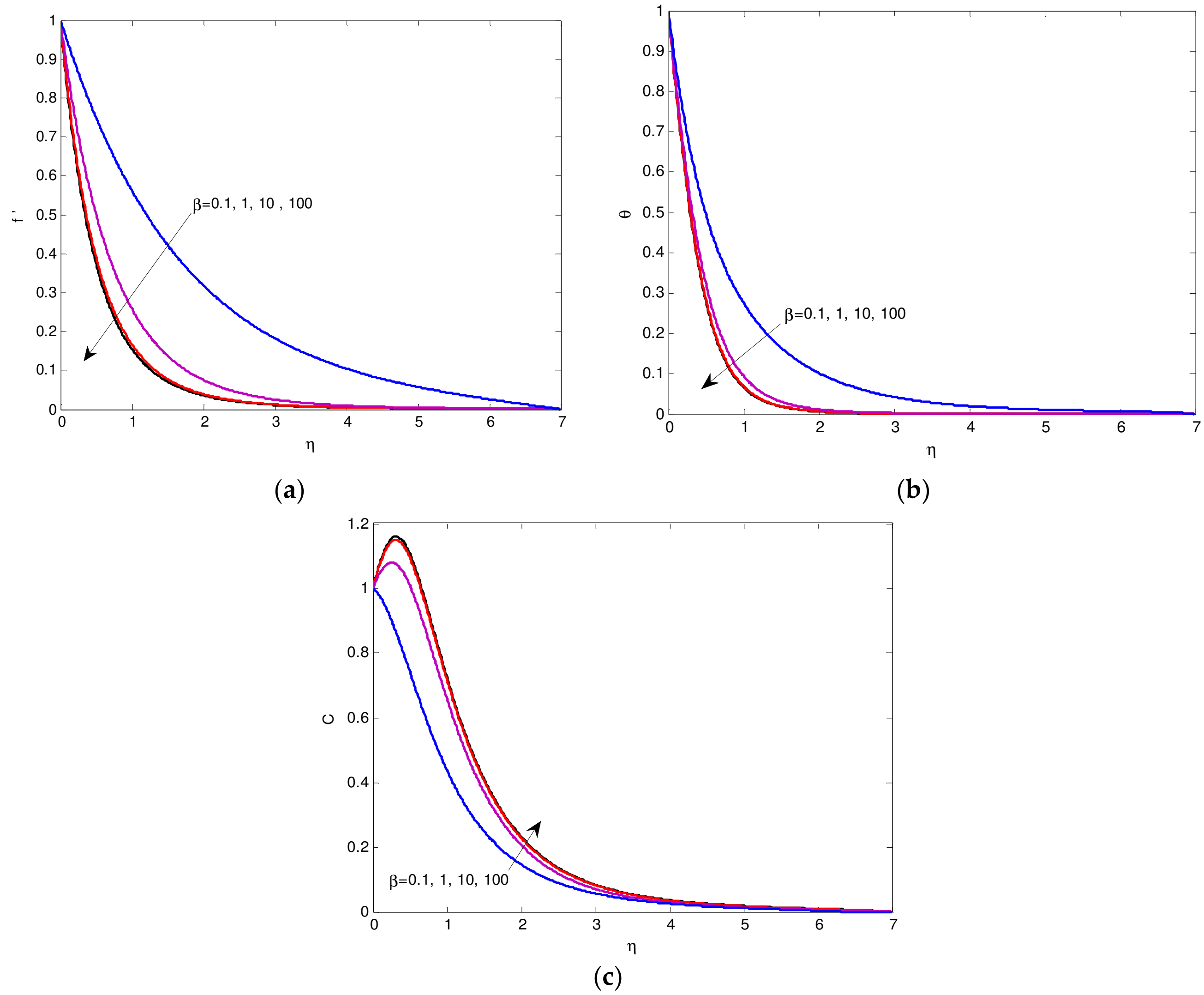

Figure 2. (**a**) The velocity f' for β values. (**b**) The temperature θ for β values. (**c**) The mass concentration C for β values.

The influence of the Schmidt parameter is given graphically in Figure 6a–c. It is found that the increase in the Schmidt parameter causes a deceleration in both the nondimensional velocity *f*\ and mass transfer. Also, the rising Sc values cause a decrease in the temperature, but the opposite effect happens rapidly far from the wall. The impact of the porous medium parameter is introduced in Figure 7a–c. It is shown that the increase in porous medium factor *K* results in raising the temperature and concentration of the nanofluid; on another hand, opposite effects are given with the nondimensional velocity *f*\ and the concentration far from the wall. The effect of the Eckert number is presented in Figure 8a–c. It is noticed that the increment in Eckert number increases both the nondimensional velocity *f*\ and the temperature. Also, the rising *Ec* causes a deceleration in the concentration, but the inverse effect is placed quickly far from the wall.

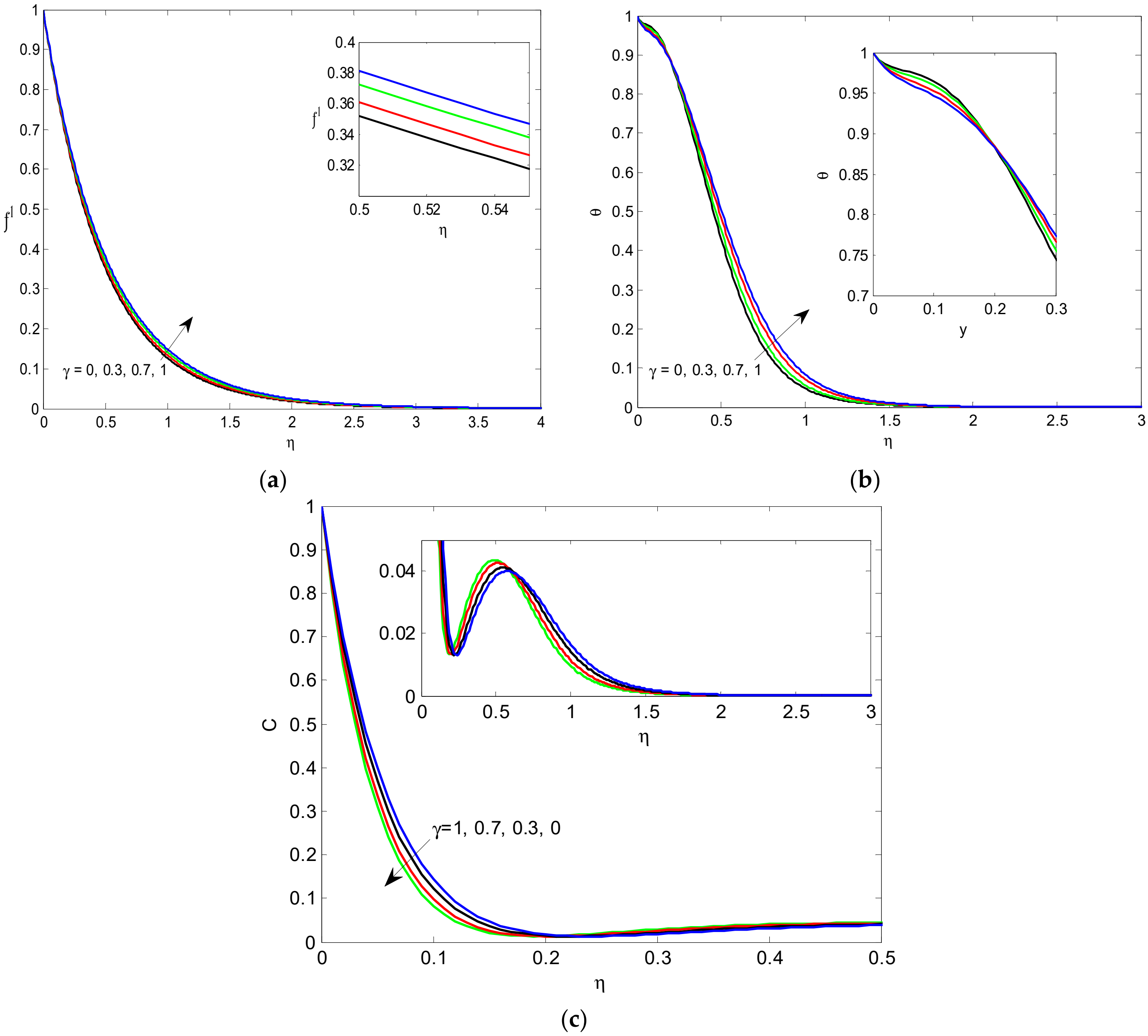

Figure 3. (**a**) The velocity f' for γ values. (**b**) The temperature θ for γ values. (**c**) The mass transfer C for γ values.

The impact of the m and n power parameters is presented in Figures 9 and 10. It is shown that the increase in the power m or the power n causes a deceleration in the nondimensional velocity $f^{\backslash}$, the temperature profiles, and the concentration distributions. The effect of heat generation is presented in Figure 11a–c. It is found that the increase in heat generation λ causes increases in both the nondimensional velocity $f^{\backslash}$ and the temperature. The growth of the heat generation results in a decrease in the concentration, but the opposite effect is placed far from the wall. The impact of the chemical reaction is shown in Figure 12. It is noted that the increase in the chemical reaction factor leads to deceleration in the mass concentration.

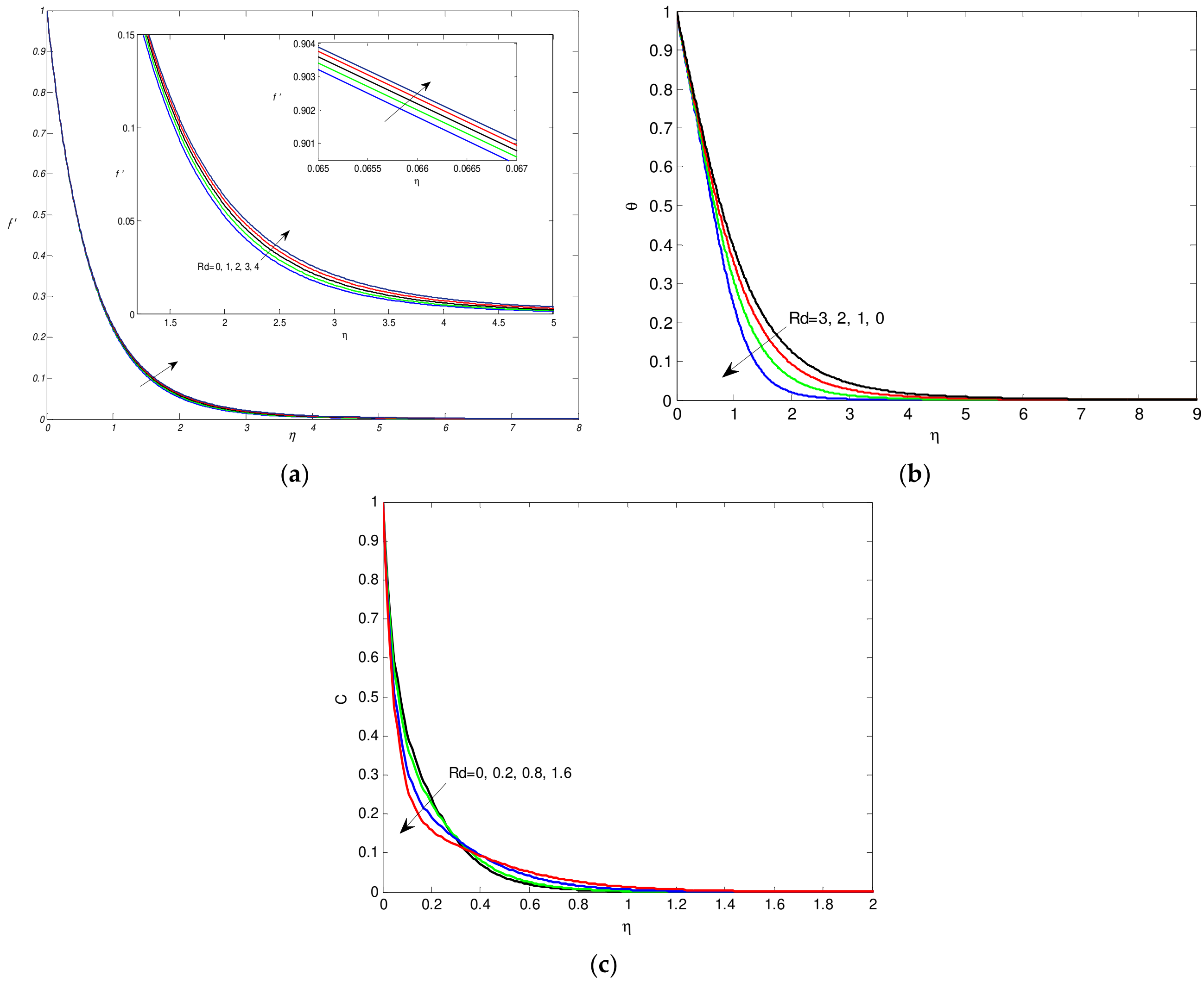

Figure 4. (**a**) The velocity f' for Rd values. (**b**) The temperature θ for Rd values. (**c**) The mass transfer C for Rd values.

Table 2 illustrates the impacts of the surface's thickness, Casson parameter, Schmidt number, Magnetic field on shear stress, and the heat flux and mass flux with the values of the involved parameters $Pr = 10$, $\beta = 0.5$, $At = 0.1$, $Nt = 0.5$, $fw = 1$, $Sc = 10.0$, $Rd = 0.5$, $\lambda = 0.2$, $\alpha = 0.5$, $Rc = 0.2$, $K = 0.2$, $Ec = 0.5$, $Nb = 0.5$, $\gamma = 0.1$, $m = 1$, $n = 1$. It is shown that the growth in the surface's thickness parameter causes an increase in the Nusselt number, but a decrease in both the shear stress and mass flux is placed. Also, it is noted that the rising values in the Casson parameter cause an increase in values for the skin friction and Nusselt number, but the opposite effect on the Sherwood Number occurred.

Also, it is noted in Table 2 that the rising Schmidt factor causes an increase in shear stress, heat flux, and mass flux. This is due to the nanofluid with increasing values of Schmidt number has a relatively low diffusion coefficient, which reduces mass diffusion and, as a result, increases the mass transfer rate at the surface. It is found that the increment in the magnetic field parameter causes a decrease in both shear stress and mass flux, but an increase in the heat flux happened. This behavior is acceptable with the physical observation that the application of transverse magnetic field results in Lorentz force, which tends to resist the fluid flow and thus reduces the fluid motion significantly.

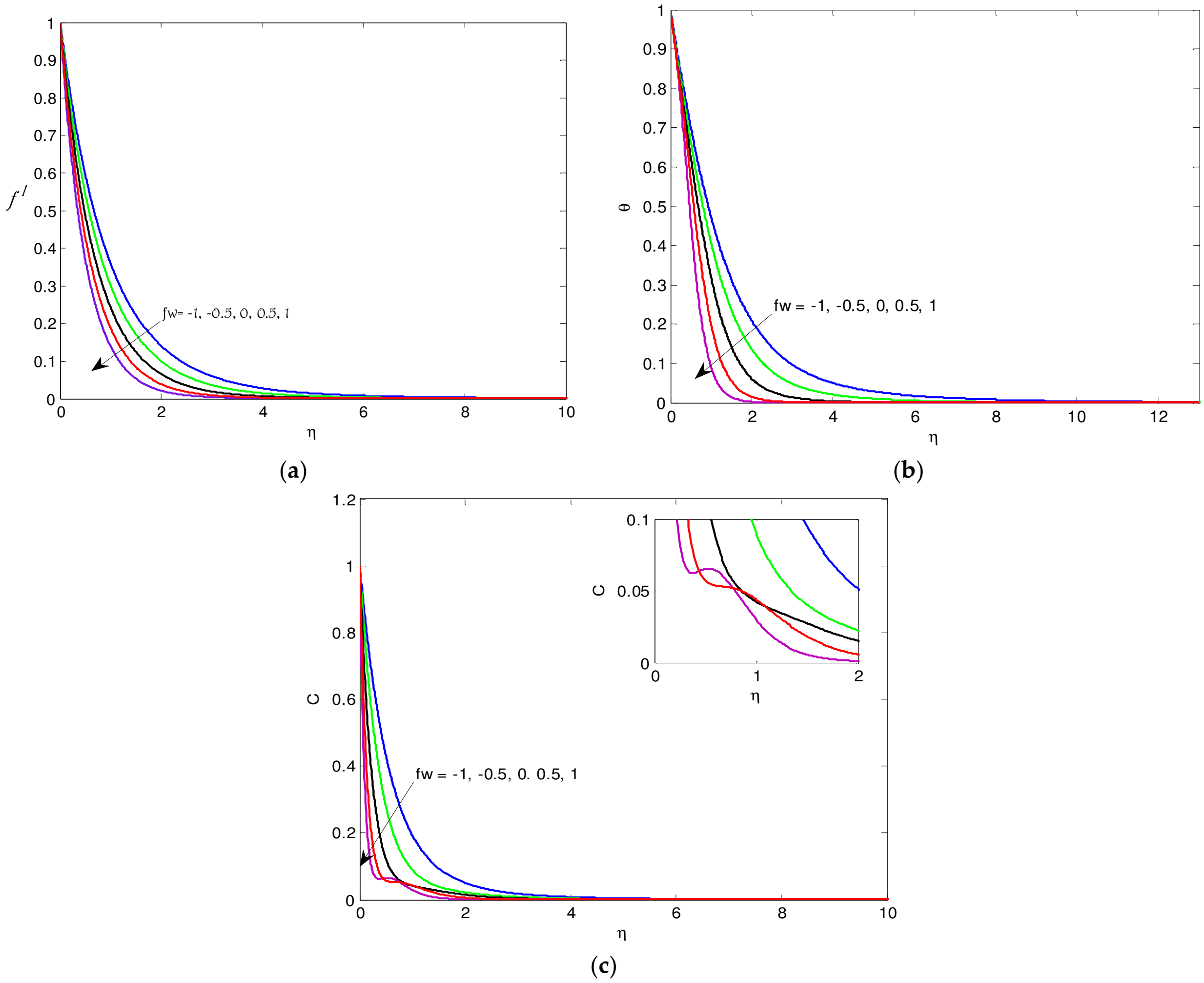

Figure 5. (**a**) The velocity for *fw* values. (**b**) The temperature θ for *fw* values. (**c**) The mass transfer C for *fw* values.

Table 2. The effect of surface variable thickness, Casson parameter, Schmidt number, Magnetic field.

$Pr = 10$, $\beta = 5$, $At = 0.1$, $Nb = 0.5$, $\phi = 0.05$, $fw = 1$, $M = 1.0$, $Rd = 0.5$, $\lambda = 0.2$, $\delta = 0.2$, $\gamma = 0.5$, $\alpha = 0.5$, $Rc = 0.2$, $K = 0.2$, $Ec = 0.5$, $Nt = 0.5$, $m = 1$, $Sc = 10.0$, $n = 1$.						
γ	β	Sc	M	$-f''(0)$	$-\theta'(0)$	$-C'(0)$
0	5	10	1.0	1.896675	2.256345	4.787477
0.5				1.878542	2.228124	4.715303
1				1.860481	2.200052	4.643463
1.5				1.842493	2.172133	4.571964
2				1.824579	2.144371	4.500815
0.5	0.5	10	1.0	1.824765	0.02412134	6.678931
	1			1.85813	1.453518	5.398466
	2			1.871352	1.961246	4.950035
	5			1.878542	2.228124	4.715303
0.5	0.5	5	1.0	1.878542	2.228124	4.715303
		10		1.920071	2.655981	9.524478
		15		1.935082	2.916045	14.31092
		20		1.942566	3.09288	19.10896
0.1	0.5	10	0.2	1.403348	1.917512	0.3306047
			1	1.704235	1.632986	0.5422387
			2	2.019402	1.273092	0.8306606
			3	2.290982	0.9057231	1.140812

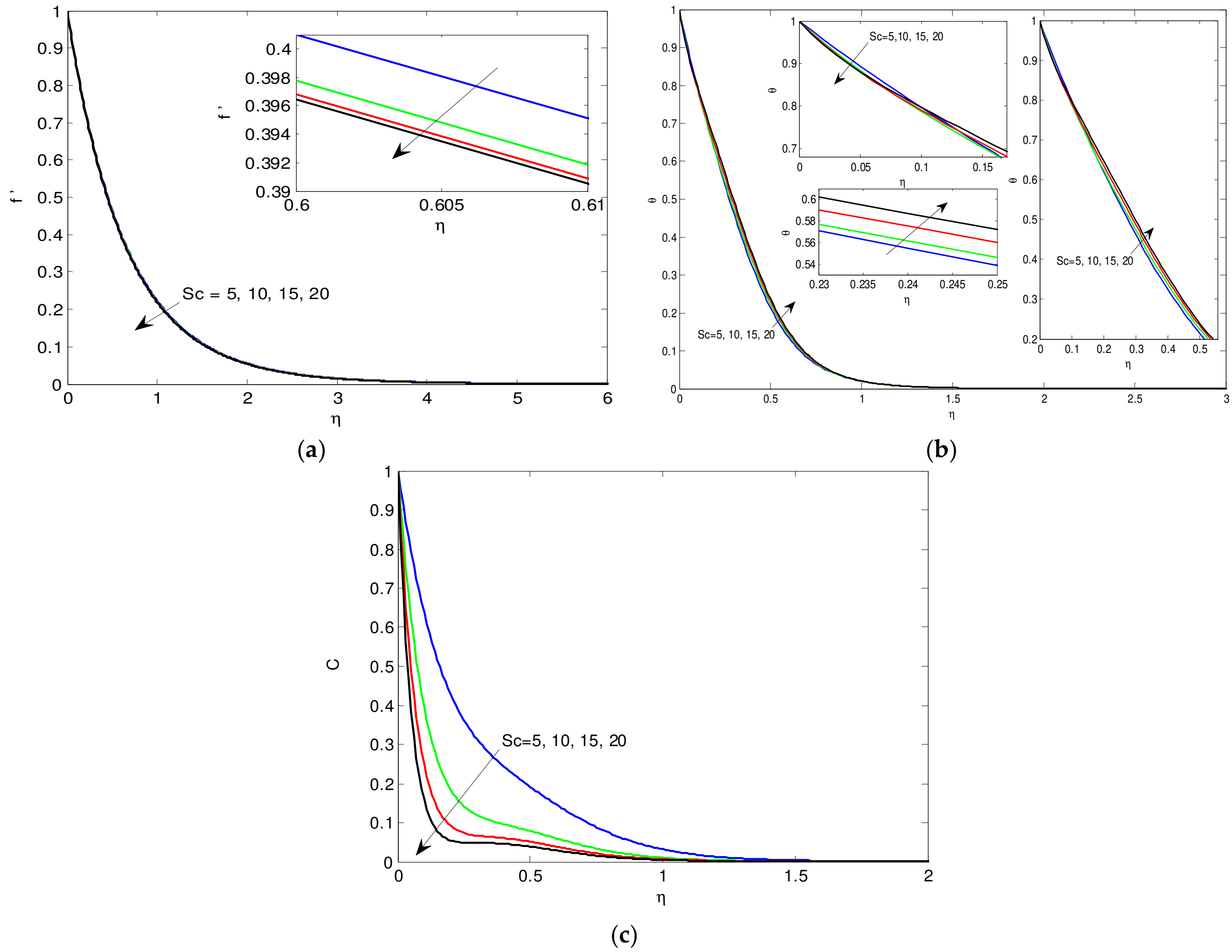

Figure 6. (**a**) The velocity via Sc. (**b**) The temperature θ for Sc values. (**c**) The mass transfer C for Sc values.

The impact of thermal radiative heat, chemically reactive flow, and nanoparticles volume on skin friction, heat flux, and mass flux are presented in Table 3. It is noted that the increment in the parameter of thermal radiation results in an increase in the Sherwood number, but a decrease in values of the skin friction and Nusselt number happened. Also, it is found from Table 4 that the increment in the nanoparticles volume causes growth in the skin friction and Sherwood number, but the inverse effect occurs in the Nusselt number, and it is noted that the acceleration in the chemical reaction results in an increase in the skin friction, heat flux, and mass flux. The influence of the parameters permeability *fw* is shown in Table 4, it is found that the increment in permeability factor causes an increase in shear stress, heat flux, and mass flux. Also, it is found that the increment in porosity factor K causes an increase in both the shear stress and mass flux, but a decrease in the heat flux is reported. It is noted that the increase in Eckert Ec leads to a fall in values of the shear stress and heat flux, but the increment in mass flux occurred. Also, it is noted from Table 4 that the rise in the power m or the power n causes increasing in shear stress, heat flux, and mass flux.

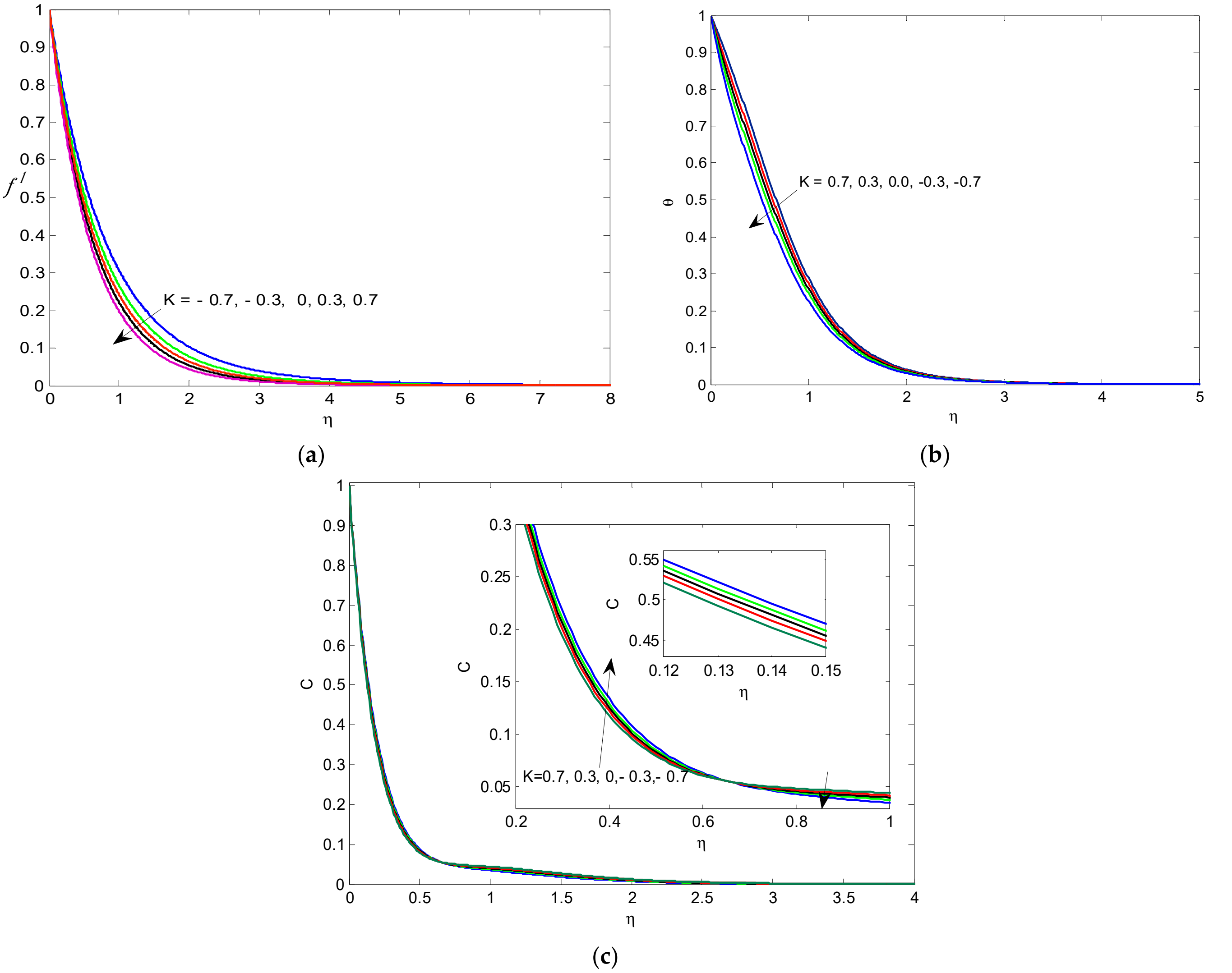

Figure 7. (**a**) The velocity via *K*. (**b**) The temperature *θ* for *K* values. (**c**) The mass transfer C for *K* values.

Table 3. The effect of thermal radiation Rd, nanoparticles volume, chemical reaction parameters.

Pr = 6.2, β = 2, A = 0.8, f_w = 2, Sc = 10.0, λ = 0.5, α = 0.5, δ = 0.2, Rc = 0.3, K = 0.2, Ec = 0.5, Nt = 0.2, Nb = 0.1, γ = 0.5, m = 1, n = 2, M = 3					
Rd	ϕ	Rc	$-f''(0)$	$-\theta'(0)$	$-C'(0)$
0	0.05	0.3	2.97296	4.770681	12.2837
0.2			2.969926	4.239647	13.26994
0.8			2.961826	3.223742	15.12073
1.6			2.952785	2.49741	16.40074
0.8	0		2.699535	3.260639	15.0950
	0.05		2.864129	3.338922	14.9355
	0.1		2.964379	3.494682	14.63177
	0.15		3.004126	3.698014	14.24473
	0.2		2.989678	3.922428	13.82292
0.8	0.05	0	2.86105	3.082186	15.0847
		1	2.864047	3.100647	18.95979
		2	2.86548	3.110097	21.52028
		3	2.866947	3.120559	25.26479
		4	2.86861	3.134327	32.89318

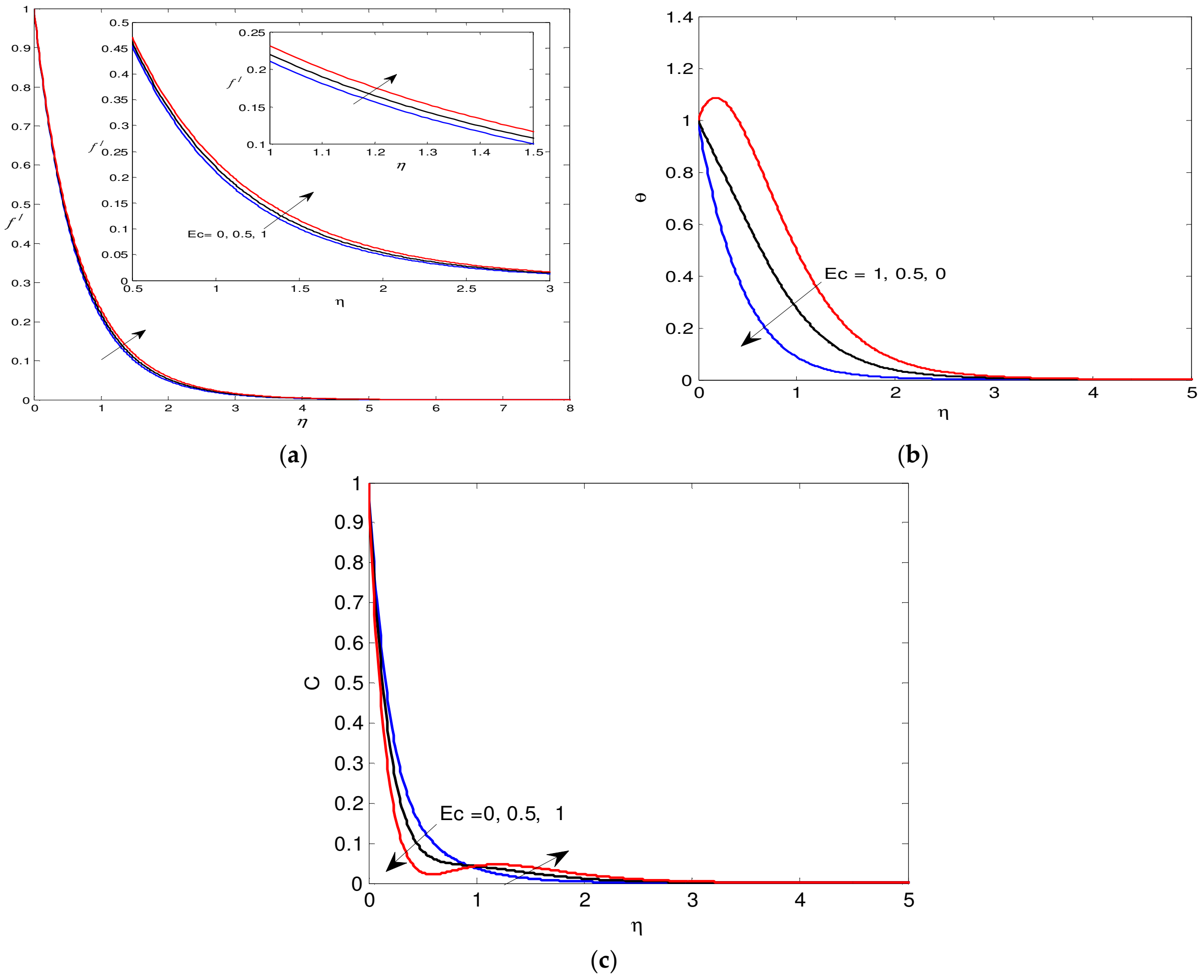

Figure 8. (**a**) The velocity via Ec. (**b**) The temperature for Ec values. (**c**) The mass transfer C for Ec values.

Table 4. The impacts of *fw*, K, Ec, the powers m, and n parameters.

***Pr* = 7, *β* = 0.5, *A* = 0.1, *Nt* = 0.5, *Nb* = 0.5, *Sc* = 10.0, *Rd* = 0.5, λ = 0.2, α = 0.2, *Rc* = 0.2, ϕ = 0.05, γ = 0.5, *M* = 1, f_w = 0.2, *K* = 0.3, Ec = 0.5**							
fw	K	Ec	m	n	$-f''(0)$	$-\theta'(0)$	$-C'(0)$
−0.7	0.3	0.5	1	2	1.166979	0.6896947	2.128103
−0.5					1.244454	0.725028	2.530241
0					1.466949	0.8371657	4.175094
0.5					1.729128	0.9243421	7.03585
0.7					1.844753	0.9296373	8.493711
0.2	−0.7				1.221034	1.467047	4.862795
	−0.3				1.369453	1.234478	4.976422
	0				1.471461	1.05878	5.069695
	0.3				1.567185	0.8816247	5.169064
	0.7				1.686805	0.6427757	5.310168
	0.3	0			1.586038	2.333166	4.397425
		0.5			1.567185	1.357548	5.169064
		0.7			1.558611	0.8816247	5.612531
		1			1.544367	0.1232255	6.556958
		0.5	1		1.567185	0.8816247	5.169064
			2		1.576039	1.405037	5.738256
			3		1.582981	1.834487	6.289898
			2	1	1.566207	1.088665	5.366438
				2	1.576039	1.405037	5.738256
				3	1.582743	1.671965	6.084604

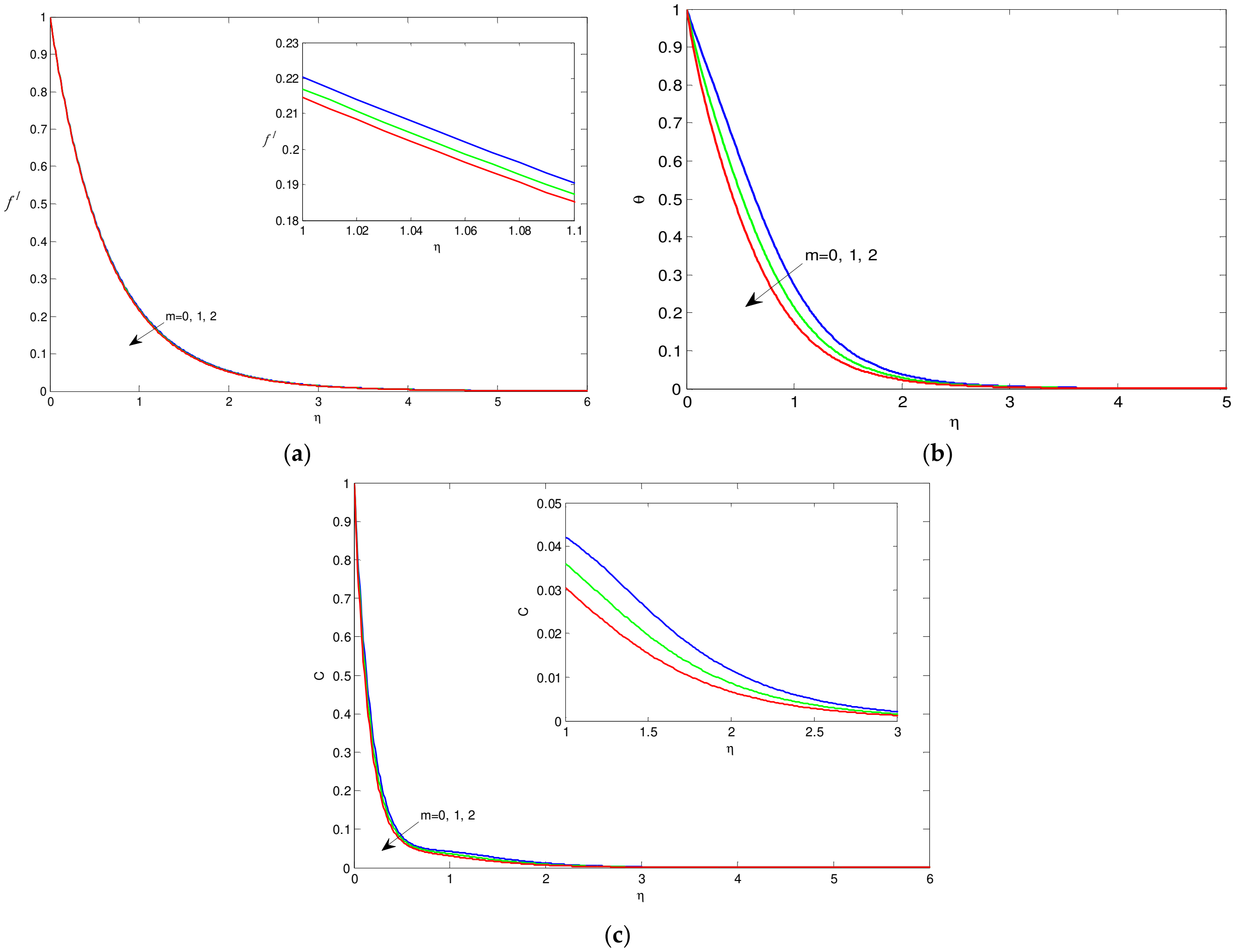

Figure 9. (**a**) The velocity via m. (**b**) The temperature for m values. (**c**) The mass transfer C for m values.

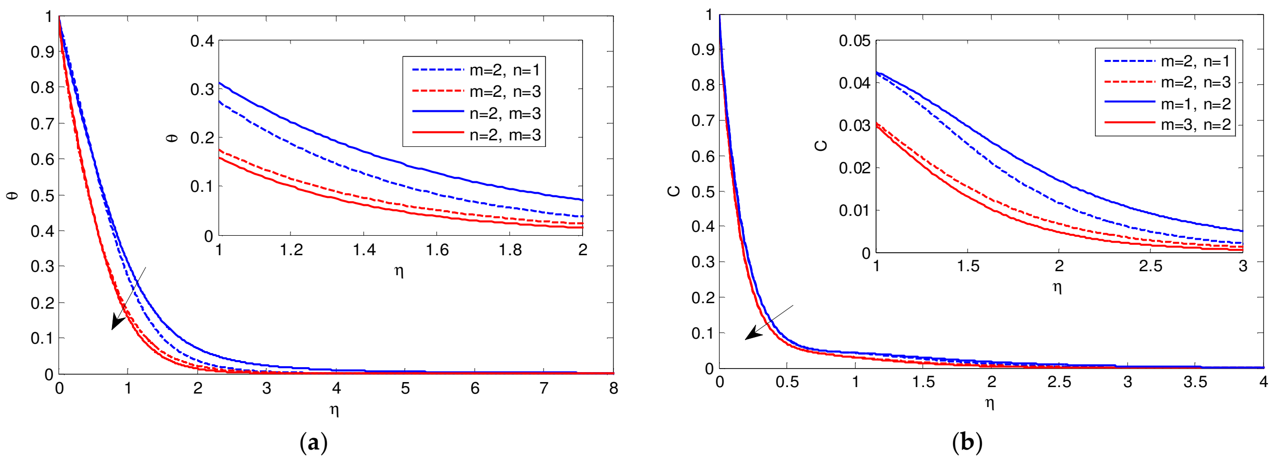

Figure 10. (**a**) The temperature θ for m and n values. (**b**) The mass transfer C for m and n values.

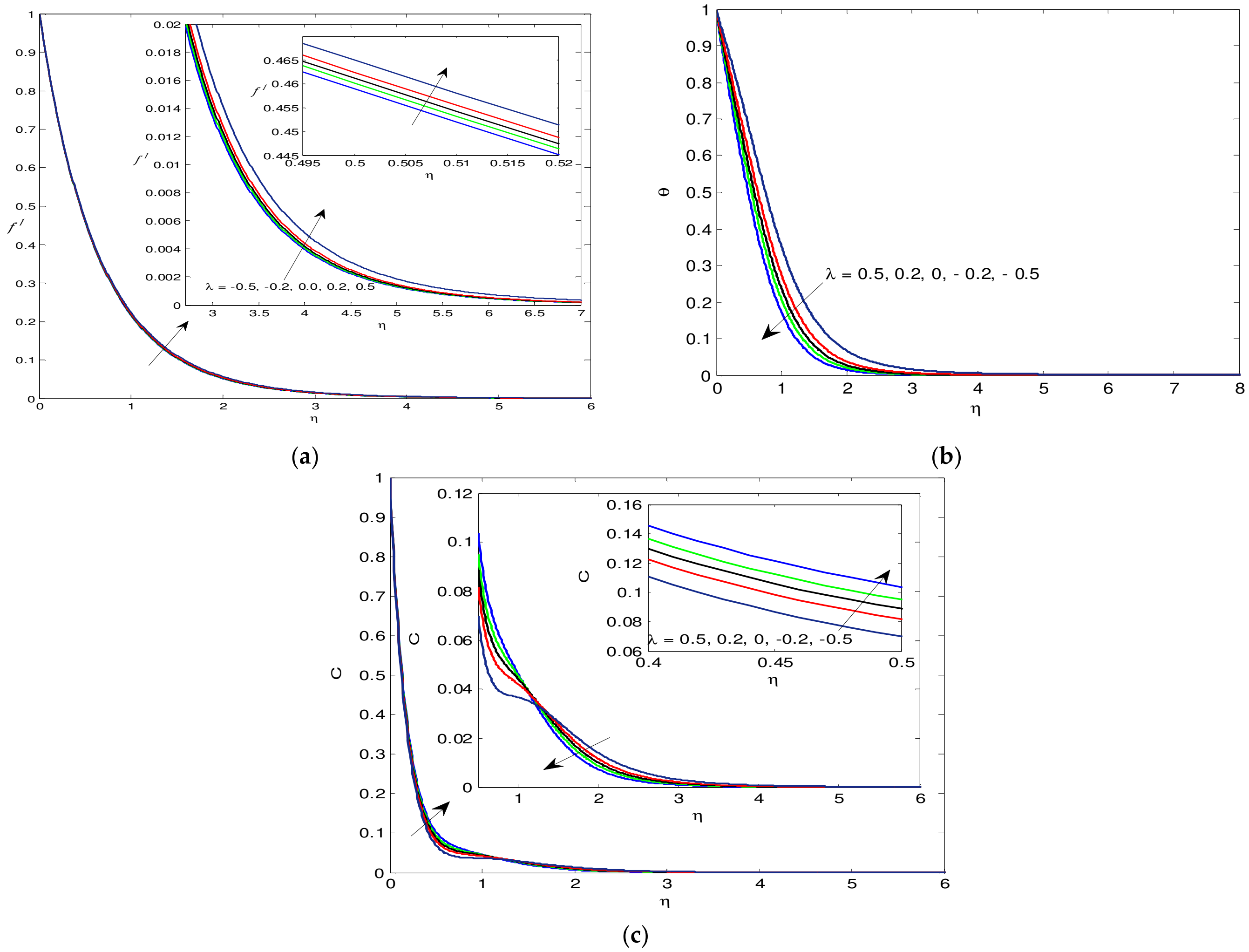

Figure 11. (**a**) The velocity via λ values. (**b**) The temperature for λ values. (**c**) The mass transfer C for λ values.

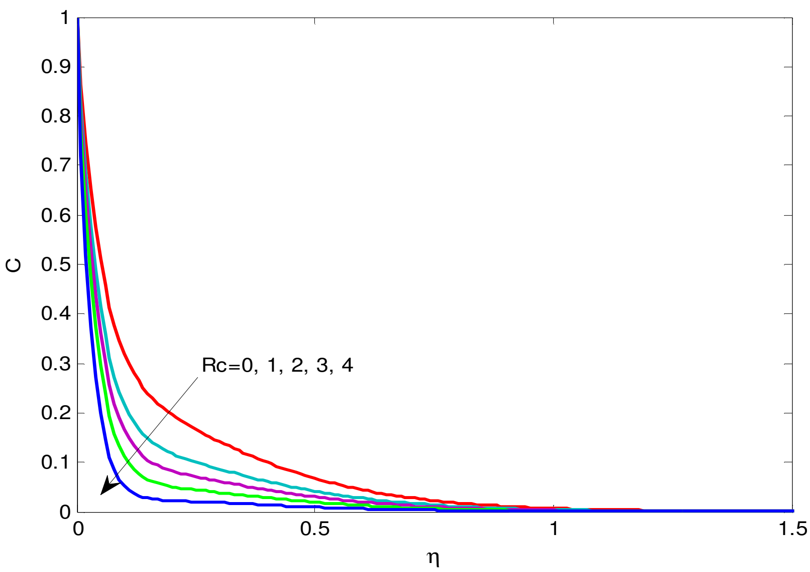

Figure 12. The mass transfer **C** for Rc values.

4. Conclusions

In the current study, the impacts of thermal radiative heat and chemically reactive flow of unsteady MHD electrically conducting Casson nanofluid over the porous stretchable surface with variable thickness immersed in a porous medium is investigated in considering heat generation, thermophoretic forces, and Brownian motion. The controlling equations are converted into nondimensional forms containing many significant physical parameters. The influence of the involved parameters is discussed and it can be summarized as follows:

The shear stress is directly proportional to the Casson parameter β, permeability factor *fw*, Schmidt number Sc, nanoparticles volume, chemical reaction *Rc*, the powers *m*, and *n* but the opposite effect occurs with, the surface's thickness variable γ, thermal radiative heat, the magnetic field, and Eckert number.

The heat flux is directly proportional to the Casson parameter β, the magnetic field M, permeability factor *fw*, Schmidt number Sc, nanoparticles volume, chemical reaction, the powers *m*, and *n*, but the opposite results occur with the surface's thickness variable γ, thermal radiation Rd, porosity factor K, and Eckert number Ec.

The concentration rate increases with the accelerated values of thermal radiation Rd, permeability factor *fw*, porosity factor K, Schmidt number Sc, chemical reaction, the distance power *m*, and the time power *n*, but the inverse effect occurs with Casson parameter β, surface's thickness variable γ, Eckert number Ec, the magnetic field M, and nanoparticles volume.

The nanofluid velocity accelerates with the growth of the thermal radiation Rd, surface's thickness variable γ, Eckert number Ec, and the heat generation factor λ, but the opposite results happen with the permeability parameter *fw*, Schmidt number, porosity factor K, distance power *m*, and time power *n* factors.

The nanofluid temperature is directly proportional to the thermal radiation Rd, porosity factor K, Eckert number Ec, and heat generation factor λ, but inversely with Casson parameter β, permeability parameter *fw*, the distance power *m*, and the time power *n*.

The fluid concentration is directly proportional to the surface's thickness variable γ, and the Casson parameter, but inversely with the permeability *fw*, Schmidt number, the porosity K, the Eckert number Ec, chemical reaction, the distance power *m*, and time power *n*.

Author Contributions: Conceptualization, A.M.S.; Software, A.M.S.; Validation, A.M.S.; Formal analysis, R.Q.; Investigation, A.M.S.; Resources, R.Q.; Writing—original draft, R.Q.; Writing—review & editing, A.M.S. All authors have read and agreed to the published version of the manuscript.

Funding: The authors extend their appreciation to the Deanship of Scientific Research, Jazan University for supporting this research work through the Research Units Support Program, Support Number: RUP2-02.

Data Availability Statement: Data are contained within the article.

Conflicts of Interest: The authors declare that there is no conflict of interest.

Nomenclature

C_f	local skin-friction coefficient ($N{\cdot}m^{-2}$)
C_p	specific heat at constant pressure (J/kg·K)
Gr	Grashof number (-)
g	acceleration due to gravity ($m\ s^{-2}$)
B	strength of the magnetic field (Tesla)
k_f	thermal conductivity of the fluid (W/m K)
k_s	thermal conductivity of the solid (W/m K)
Ec	Eckert number (-)
K	porosity parameter (-)
Nt	thermophoretic parameter
Nb	Brownian motion parameter
Sc	Schmidt number (-)

fw	surface flow flux parameter (-)
Rc	Chemical reaction parameter
M	magnetic parameter (-)
N_T	temperature ratio parameter (-)
Nu	local Nusselt number (-)
Pr	Prandtl number (-)
q_r	radiative heat flux (W/m^2)
Rd	radiative parameter (-)
Re	Reynolds number (-)
Shx	Sherwood number (-)
Q	heat generation coefficient ($J/m^2 \cdot K \cdot s$)
T_f	temperature of the fluid (K)
q_w	surface heat flux (w/m^2)
q_c	mass flux ($kg/m^2 \cdot s$)
T_∞	temperature of the ambient fluid (K)
T_w	temperature at the surface (K)
(u, v)	fluid velocities in the x, y-directions (ms^{-1})
(x, y)	axis direction (m)
Greek symbols	
ψ	stream function ($kg/m \cdot s$)
Θ	nanofluid dimensionless temperature (-)
Φ	nanofluid dimensionless concentration (-)
τ_w	shearing stress (N/m^2)
ρ	density of the fluid ($kg\ m^{-3}$)
μ	dynamic viscosity of the fluid ($N\ s/m^2$)
v	kinematic viscosity ($N\ s/m^2$)
γ	thermal variation parameter ($W/m^3 \cdot K$)
α	conjugate conduction heat parameter
θ	dimensionless temperature (-)
λ	heat generation factor (-)
ϕ	volume fraction (-)
β	coefficient of thermal expansion (1/K)
η	space variable (-)
Subscripts	
w	wall conditions
∞	ambient temperature
Superscript	
\	differentiation with respect to y

References

1. Keller, H.B. Numerical Methods in Boundary Layer Theory. *Annu. Rev. Fluid Mech.* **1978**, *10*, 417–433. [CrossRef]
2. Cebeci, T.; Bradshaw, P. *Physical and Computational Aspects of Convective Heat Transfer*; Springer: New York, NY, USA, 1984.
3. Elbashbeshy, E.M.A.; Bazid, M.A. Heat transfer over an unsteady stretching surface. *Heat Mass Transf.* **2004**, *41*, 1–4. [CrossRef]
4. Ishak, A. Unsteady MHD flow and heat transfer over a stretching sheet. *J. Appl. Sci.* **2010**, *10*, 2127–2131. [CrossRef]
5. Ibrahim, W.; Shanker, B. Unsteady MHD boundary layer flow and heat transfer due to stretching sheet in the presence of heat source or sink. *Comput. Fluids J.* **2012**, *70*, 21–28. [CrossRef]
6. Makinde, O.D.; Khan, W.A.; Gulham, J.R. MHD variable viscosity reacting flow over a convectively heated plate in a porous medium with thermophoresis and radiative heat transfer. *Int. J. Heat Mass Transf.* **2016**, *93*, 595–604. [CrossRef]
7. Sheikholeslami, M. Numerical simulation of magnetic nanofluid natural convection in porous media. *Phy. Lett. A.* **2017**, *381*, 494–503. [CrossRef]
8. Elbashbeshy, E.M.A.; Eldabe, N.T.M.; Sedki, A.M. Effects of pressure stress work and thermal radiation on free convection flow around a sphere embedded in a porous medium with Newtonian heating. *Therm. Sci.* **2018**, *22*, 401–412. [CrossRef]
9. Eldabe, N.T.M.; Ghaly, A.Y.; Mohamoud, M.S.H. MHD boundary layer chemical reacting flow with heat transfer of Eyring-Powell nanofluid past a stretching sheet. *Microsyst. Technol.* **2018**, *24*, 4945–4953. [CrossRef]
10. Trivedi, M.; Ansari, M.S.; Motsa, S.S. Flow and heat transfer of a nanofluid by mixed convection with non-uniform heat source/sink and magnetic field effect: A numerical approach. *Comput. Therm. Sci.* **2019**, *11*, 189–203.
11. Mahabaleshwar, U.S.; Nagaraju, K.R.; Lorenzini, G. Effect of mass transfer and MHD induced Navier's slip flow due to non-linear stretching sheet. *J. Eng. Thermophyscis* **2019**, *28*, 578–600. [CrossRef]

12. Khan, A.; Naem, S.; Vafai, K. Dufour, and Soret effects on Darcy-Forchheimer flow of second-grade fluid with the variable magnetic field and thermal conductivity. In *International Journal of Numerical Methods for Heat and Fluid Flow*; Emerald Publishing Limited: Bingley, UK, 2019; ISSN 0961-5539. [CrossRef]
13. Maleki, H.; Alsarraf, J.; Safaei, M.R. Heat transfer and nanofluid flow over a porous plate with radiation and slip boundary conditions. *J. Cent. South Univ.* **2019**, *26*, 1099–1115. [CrossRef]
14. Pordanjani, A.H.; Aghakhani, S.; Afrand, M. Investigation of free convection heat transfer entropy generation of nanofluid flow inside a cavity affected by a magnetic field and thermal radiation. *J. Therm. Anal. Calorim.* **2019**, *137*, 997–1019. [CrossRef]
15. Chaudhary, S.; Kanika, K.M. Heat generation/absorption and radiation effects on hydromagnetic stagnation point flow of nanofluids toward a heated porous stretching/shrinking sheet with suction/injection. *J. Porous Medium* **2020**, *23*, 27–49. [CrossRef]
16. Reddy, P.S.; Sreedevi, P. MHD boundary layer heat and mass transfer flow of nanofluid through porous media over an inclined plate with chemical reaction. *Multidiscip. Model Mater Struct* **2021**, *17*, 317–336. [CrossRef]
17. Eldabe, N.T.M.; Abou-Zeid, M.Y.; Mohamed, M.A.A. MHD peristaltic non-Newtonianewtonian power-law nanofluid through a non-Darcy porous medium inside a non-uniform inclined channel. *Arch. Appl. Mech.* **2021**, *91*, 1067–1077. [CrossRef]
18. Sedki, A.M.; Abo-Dahab, S.M.; Bouslimi, J.; Mahmoud, K.H. Thermal radiation effect on unsteady mixed convection boundary layer flow and heat transfer of nanofluid over permeable stretching surface through a porous medium in the presence of heat generation. *Sci. Prog.* **2021**, *104*, 1–19. [CrossRef]
19. Sedki, A.M. Effect of thermal radiation and chemical radiation on MHD mixed convective heat and mass transfer in nanofluid flow due to a nonlinear stretching surface through a porous medium. *Results Mater.* **2022**, *16*, 100334. [CrossRef]
20. Mukhopadhyay, S. Effects of thermal radiation on Casson fluid flow and heat transfer over an unsteady stretching surface subjected to suction/blowing. *Chin. Phys. B* **2013**, *22*, 114702. [CrossRef]
21. Makanda, G.; Shaw, S.; Sibanda, P. Diffusion of chemically reactive species in Casson fluid flow over an nsteady stretching surface in porous medium in the presence of a magnetic field. *Math. Probl. Eng.* **2015**, *2015*, 724596. [CrossRef]
22. Raju, C.S.K.; Sandeep, N.; Reddy, J.V.R. Heat and mass transfer in magnetohydrodynamic Casson fluid over an exponentially permeable stretching surface. *Eng. Sci. Technol.* **2016**, *19*, 45–52. [CrossRef]
23. Oyelakin, I.S.; Mondal, S.; Sibanda, P. Unsteady Casson nanofluid flow over a stretching sheet with thermal radiation, convective and slip boundary conditions. *Alex. Eng. J.* **2016**, *55*, 1025–1035. [CrossRef]
24. Krishnamurthy, M.R.; Gireesha, B.J.; Gorla, R.S.R. Thermal radiation and chemical reaction effects on boundary layer slip flow and melting heat transfer of nanofluid induced by nonlinearly stretching sheet. *Nonlinear Eng.* **2016**, *5*, 147–159. [CrossRef]
25. Ullah, I.; Bhattacharyya, K.; Shafie, S.; Ilyas Khan, I. Unsteady MHD mixed convection slip flow of Casson fluid over nonlinearly stretching sheet embedded in a porous medium with chemical reaction, thermal radiation, heat generation/absorption, and convective boundary conditions. *PLoS ONE* **2016**, *11*, 0165348. [CrossRef] [PubMed]
26. Prasad, K.V.; Vajravelu, K.; Vaidya, H. MHD Casson nanofluid flow and heat transfer at a stretching sheet with variable thickness. *J. Nanofluids* **2016**, *5*, 423–435. [CrossRef]
27. Tamoor, M.; Waqas, M.; Khan, M.I.; Alsaedi, A.; Hayat, T. Magnetohydrodynamic flow of Casson fluid over a stretching cylinder. *Results Phys.* **2017**, *7*, 498–502. [CrossRef]
28. Naqvi, S.M.R.S.; Muhammad, T.; Asma, M. Hydromagnetic flow of Casson nanofluid over a porous stretching cylinder with Newtonian heat and mass conditions. *Phys. A* **2020**, *550*, 123988. [CrossRef]
29. Shit, G.C.; Mandal, S. Entropy analysis on unsteady MHD flow of Casson nanofluid over a stretching vertical plate with thermal radiation effect. *Int. J. Appl. Comput. Math.* **2020**, *6*, 2. [CrossRef]
30. Krishna, M.V.; Ahammad, N.A.; Chamkha, A.J. Radiative MHD flow of Casson hybrid nanofluid over an infinite exponentially accelerated vertical porous surface. *Cas Stud. Therm. Eng.* **2021**, *27*, 101229. [CrossRef]
31. Bejawada, S.G.; Reddy, Y.D.; Jamshed, W.; Nisar, K.S.; Alharbi, A.N.; Chouikh, R. Radiation effect on MHD Casson fluid flow over an inclined non-linear surface with chemical reaction in a Forchheimer porous medium. *Alex. Eng. J.* **2022**, *61*, 8207–8220. [CrossRef]
32. Sedki, A.M. Computational analysis of MHD Cross nanofluid containing gyrotactic microorganisms over permeable horizontal cylinder through a porous medthe ium in presence of thermal radiation and chemical reaction. *Partial Differ. Equ. Appl. Math.* **2023**, *7*, 100508. [CrossRef]
33. Khan, M.N.; Ahmad, S.; Wang, Z.; Fadhl, B.M.; Irshad, K. Enhancement in the efficiency of heat recovery in a Williamson hybrid nanofluid over a vertically thin needle with entropy generation. *Heliyon* **2023**, *9*, 17665. [CrossRef] [PubMed]